Conformation of Arborescent Polymers in Solution by Small-Angle Neutron Scattering: Segment Density and Core−Shell Morphology

Seok Il Yun,*,†,‡ Kai-Chi Lai,§ Robert M. Briber,§ Steven J. Teertstra,|| Mario Gauthier,|| and Barry J. Bauer⊥

Institute for Environmental Research, Australian Nuclear Science & Technology Organization, PMB 1, Menai, NSW 2234, Australia, Center for Neutron Scattering, Oak Ridge National Laboratory, Oak Ridge, Tennessee 37831, Department of Materials Science and Engineering, University of Maryland, College Park, Maryland 20742, Department of Chemistry, Institute for Polymer Research, University of Waterloo, Waterloo, Ontario N2L 3G1, Canada, and Polymers Division, National Institute of Standards and Technology, Gaithersburg, Maryland 20899-8541

Received September 19, 2007; Revised Manuscript Received November 12, 2007

ABSTRACT: The radius of gyration (R_g) was determined as a function of generation number for arborescent polystyrenes with two different side chain mass average molecular mass ($M_w \approx 5000$, 5K, versus 30 000, 30K) by small-angle neutron scattering (SANS) measurements. The R_g values obtained were analyzed in terms of the Zimm−Stockmayer model for randomly branched polymers, the scaling relation $R_g \propto M_w^{\upsilon}$, and the expansion factor $\alpha_s = (R_g)_{goodsolvent}/(R_g)_{\Theta solvent}$. The R_g and scaling exponent $\upsilon = 0.26 \pm 0.01$ found for G0 through G3 polymers with 5K side chains in cyclohexane-*d* correspond to the values predicted by the Zimm−Stockmayer model. The R_g for G0 through G3 polymers with 30K side chains deviate from the model with $\upsilon = 0.32 \pm 0.02$, corresponding to $\upsilon = 0.33$ expected for hard spheres. Deuterated polystyrene (PS-*d*) side chains were grafted onto G2 and G3 polystyrene (PS) cores. These copolymers, G2PS-*graft*-PS-*d* and G3PS-*graft*-PS-*d*, were characterized as spheres with a well-defined PS core−PS-*d* shell structure by the SANS contrast matching method. The shape and the segment radial density profile of the core and shell for GPS-*graft*-PS-*d* were determined based on $P(r)$ and $\Delta\rho(r)$ obtained by indirect Fourier transformation and deconvolution methods ($P(r)$, pair distance distribution function and $\Delta\rho(r) = \rho(r) - \rho(\text{solvent})$, scattering length density contrast profile).

Introduction

Dendritic polymers are a class of cascade-branched molecules including dendrimers, hyperbranched polymers, and dendrigraft (or arborescent) polymers.[1−5] Dendritic polymers have generated considerable research interest in nanotechnology due to their controllable dimensions, topology, structure, and chemical functionality on the nanometric scale. The multistep synthesis and slow molecular mass growth of dendrimers is often considered to be a major drawback hindering the use of these materials on a large scale.[2,3] In contrast to dendrimers, arborescent polymers incorporate well-defined linear polymer segments rather than monomers as building blocks, which leads to cascade-branched polymers with a very high relative molecular mass in a few grafting cycles (generations), while maintaining a narrow relative molecular mass distribution ($M_w/M_n < 1.1$). The hard spherelike behavior of arborescent polymers has been investigated previously with the help of intrinsic viscosity, osmotic pressure, and differential scanning calorimetry measurements.[6,7] In the current study, we used small-angle neutron scattering (SANS) measurements to confirm the core−shell morphology of arborescent polymers and to further characterize their solution behavior. To elucidate the influence of side chain length on polymer morphology, two series of arborescent polystyrenes (PS) were used in the SANS experiments, in analogy to previous studies.[6,7] A target branching density of around 15 side chains per backbone chain and a constant side chain mass-average relative molecular mass (M_w) of either 5000 (5K) or 30 000 (30K) were used for each generation.

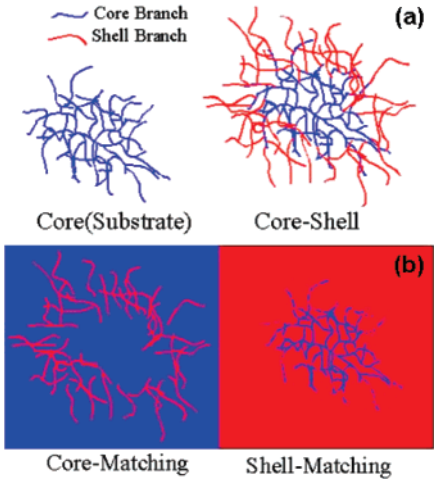

Figure 1. Schematic representation of (a) core−shell morphology of an arborescent copolymer and (b) solvent matching of the core and the shell.

The "graft-upon-graft" approach used to synthesize arborescent polymers can yield either homopolymers or copolymers with a core−shell structure (Figure 1a).[8,9] Despite substantial synthetic efforts, detailed characterization of the core−shell morphology of these materials has been elusive so far due to insufficient contrast between the core and shell polymers in neutron and X-ray scattering experiments.[10,11] For the present investigation, arborescent polymers were synthesized by grafting

* To whom correspondence should be addressed.
† Australian Nuclear Science & Technology Organization.
‡ Oak Ridge National Laboratory.
§ University of Maryland.
|| University of Waterloo.
⊥ National Institute of Standards and Technology.

10.1021/ma7021106 CCC: $40.75
Published on Web 12/12/2007

Table 1. Characteristics of Arborescent Polystyrenes with 5K and 30K Side Chains

	side chains		graft polymers	
sample	$M_w/10^3$ (SEC)[a]	M_w/M_n (SEC)[a]	M_w (LS)[b]	f_w(tot)
G0PS-5K	4.4	1.03	$(5.7 \pm 0.1) \times 10^4$	12
G1PS-5K	4.7	1.03	$(5.7 \pm 0.1) \times 10^5$	120
G2PS-5K	4.4	1.04	$(3.2 \pm 0.1) \times 10^6$	720
G3PS-5K	4.6	1.05	$(2.4 \pm 0.1) \times 10^7$	5200
G0PS-30K	25	1.10	$(4.3 \pm 0.1) \times 10^5$	17
G1PS-30K	27	1.09	$(9.0 \pm 0.2) \times 10^6$	333
G2PS-30K	27	1.09	$(1.2 \pm 0.2) \times 10^8$	4440
G3PS-30K	28	1.09	$(5 \pm 2) \times 10^8$	18 900

[a] Absolute mass-average relative molecular mass and polydispersity index from size exclusion analysis using linear polystyrene standards calibration. [b] Absolute mass-average relative molecular mass from light scattering measurements.

a deuterated polystyrene shell onto polystyrene cores, in order to apply the contrast matching method of SANS to arborescent polymers for the first time (Figure 1b). We report on the evolution of the core−shell morphology of arborescent polymers as a function of generation number (G) and solvent quality.

Experimental Procedures

The synthesis of the arborescent polymers used in this study was discussed in detail elsewhere.[6−9] Two series of arborescent polystyrenes were prepared containing side chains with a mass-average relative molecular mass (M_w) of either 5000 (5K) or 30 000 (30K) for each generation. The characteristics of these materials are summarized in Table 1. The relative molecular mass of the side chains (branches) determined by size exclusion chromatography analysis is estimated to have an attached standard uncertainty of ±5%. The total M_w of the graft polymers, determined from batchwise light scattering measurements, is also reported in Table 1 with uncertainties derived from Zimm analysis of the data. The total number of branches present in a generation G polymer was calculated according to the equation

$$f_w(\text{tot}) = f_w(G-1) + \frac{M_w(G) - M_w(G-1)}{M_w(\text{branch})} \quad (1)$$

where $M_w(G)$, $M_w(G-1)$, and M_w(branch) represent the mass-average relative molecular mass of polymers of generation G, of the previous generation, and of the side chains, respectively. To apply the SANS contrast matching method, deuterated polystyrene (PS-*d*, *d*: deuterated) side chains were grafted randomly onto G2 and G3 polystyrene (PS) cores with 5K side chains. The characteristics of the arborescent polystyrene substrates and the deuterated copolymers derived from them are provided in Tables 2 and 3, respectively. Deuterated and protonated solvents were combined to match the scattering length density (SLD) of the polymers according to $\rho_{\text{polymer}} = \phi_{v,P}\rho_{v,P} + \phi_{v,D}\rho_D$ where ρ = scattering length density, ϕ_v = volume fraction, and the subscripts P and D correspond to the protonated and deuterated solvents, respectively. When the SLD values of a solvent and core (shell) are matched, scattering arises only from the shell (core) portion of the molecules (Figure 1b). The tetrahydrofuran (THF)/THF-*d* and cyclohexane/cyclohexane-*d* solvent systems were used for the PS-*graft*-PS-*d* arborescent copolymers. One of the goals in the SANS experiments was to measure the dimensions (radius of gyration, R_g) of the polymers in dilute solutions. SANS measurements were performed for the homopolymers listed in Table 1 for dilute solutions with $\phi = 0.005$ (ϕ = mass fraction). The concentration of the solutions used for the copolymers listed in Table 3 for the contrast matching experiments was $\phi = 0.01$. On the basis of our SANS results from solutions within the concentration range ($0.005 < \phi < 0.02$), we found that R_g was almost independent of ϕ (the uncertainty on R_g due to concentration variations was below 5%).

Table 2. Characteristics of Arborescent Polystyrene Cores Used as Substrates for the Synthesis of Deuterated Copolymers

	side chains		graft polymers	
core polymer	$M_w/10^3$ (SEC)[a]	M_w/M_n (SEC)[a]	M_w (LS)[b]	f_w(tot)
G2PS	5.2	1.07	5×10^6	826
G3PS	5.9	1.08	2.2×10^7	2930

[a] Absolute mass-average relative molecular mass and polydispersity index from size exclusion analysis using linear polystyrene standards calibration. [b] Absolute mass-average relative molecular mass from light scattering measurements.

The SANS experiments were carried out at the Center for Neutron Research of the National Institute of Standards and Technology, using the 30 m NIST-NG3 and NG7 instruments.[12,13] The raw data were corrected for scattering from the empty cell, detector dark current, detector sensitivity, sample transmission, and thickness. After these corrections, the data were placed on an absolute scale using either a calibrated secondary standard or direct beam measurement and circularly averaged to produce $I(q)$ versus q plots where $I(q)$ is the scattered intensity and $q = \sin(\theta)4\pi/\lambda$ is the scattering vector for a scattering angle θ. The q range used was (0.0046−0.0820) Å^{-1} and the neutron wavelength was $\lambda = 6$ Å with a wavelength spread $\Delta\lambda/\lambda = 0.15$. Two sets of MgF_2 biconcave lenses were used to investigate samples G3PS-30K and G3PS-*graft*-PS-*d* in the very low q regime (0.0014−0.05 Å^{-1}).

The relative uncertainties reported are one standard deviation, based on the goodness of the fit or from multiple runs. Total combined uncertainties from all external sources are not reported, as comparisons are made with data obtained under the same conditions. In cases where the limits are smaller than the plotted symbols, the limits are left out for clarity.

Certain equipment, instruments, or materials are identified in this paper in order to adequately specify the experimental details. Such identification does not imply recommendation by the National Institute of Standards and Technology nor does it imply the materials are necessarily the best available for the purpose.

Results and Discussion

Radius of Gyration and Scaling Behavior of PS Arborescent Homopolymers. The SANS data collected for arborescent styrene homopolymers with 5K side chains in cyclohexane-*d* ($\phi = 0.005$) are provided as $I(q)\,q^2$ vs q (Kratky) plots in Figure 2a. Kratky plots generally show a pronounced maximum for scattering from spherical objects such as star and hyperbranched polymers. Such a maximum is observed for G1−G3 polymers, confirming that the shape of arborescent polymers in solution is spherical. Interestingly no maximum is present for the G0 polymer, with a comb-branched structure incorporating twelve 5K side chains grafted onto a 5K backbone, expected to have a more ellipsoidal shape. As the generation number increases, the scattering peak becomes more pronounced, a second maximum being apparent for the G3 polymer. Multiple peaks in the Kratky plot such as observed for the G3 polymer are characteristic of hard spheres of uniform size. The location of the maximum (q_{max}) is shifted to lower q values with increasing G. The parameter q_{max} is inversely proportional to the radius of gyration (R_g) for spherical scattering objects ($R_g \approx u/q_{max}$), the value of u for branched polymers depending on the shape of the molecules and their branching density.[14,15] Regardless of the type of object involved, R_g can be extracted from SANS data by applying the Guinier equation, $I(q) = I(0)\exp(-R_g^2q^2/3)$. The R_g values were calculated from the Guinier plots for the same solutions ($\phi = 0.005$ in cyclohexane-*d*), and the results are provided in Table 4. In combination with q_{max} derived from the Kratky plots (Figure 2a), the product $q_{max}R_g$ is almost constant and corresponds to an average value of $u = 1.733 \pm$

Table 3. Characteristics of PS-*graft*-PS-*d* Copolymers

		side chains[a]			graft copolymers	
core polymer	copolymer	M_w	M_w/M_n	graft polymer composition /mass %[b]	M_w(LS)[c]	f_w(tot)
G2PS	G2PS-*graft*-PS-*d*	4 500	1.07	85	3.1×10^7	5 800
G3PS	G3PS-*graft*-PS-*d*	4 600	1.09	81	1.3×10^8	23 000

[a] Absolute mass-average relative molecular mass and polydispersity index of PS-*d* from size exclusion analysis using linear polystyrene standards calibration. [b] Copolymer composition (mass % PS-*d*) determined from molecular mass increase. [c] Absolute mass-average relative molecular mass from light scattering measurements.

Table 4. Comparison of R_g Values Obtained for Arborescent Polystyrenes with 5K and 30K Side Chains in Cyclohexane-*d* by Different Methods

		R_g (nm)		
		measured by SANS		
sample		Guinier	Kratky	calculated Z−S model
5k	G0	4.9 ± 0.6		4.2
	G1	8.5 ± 0.2	8.6 ± 0.4	8.5
	G2	14.4 ± 0.2	14.4 ± 0.7	13.2
	G3	22.7 ± 0.1	22.5 ± 1.1	22.3
30k	G0	8.6 ± 0.1	8.3 ± 0.4	12.2
	G1	20.5 ± 1.4	20.9 ± 1.1	29.7
	G2	44.7 ± 1.2	43.3 ± 2.2	58.2
	G3	85.3 ± 0.3	86.6 ± 4.3	85.4

$0.021 \approx \sqrt{3}$ (Figure 2b). The R_g of these arborescent polymers can therefore be determined from a Kratky plot using

$$q_{max}R_g = \sqrt{3} \tag{2}$$

The form factor for hyperbranched polymers that are nonrandom AB_f-type polycondensates where group A can react only with groups B was determined by Burchard[14] as

$$P(q) = (1 + q^2R_g^2/6)^{-2} \tag{3}$$

With the use of the form factor from Burchard, the maximum in the plot of $P(q)q^2$ vs q should approach a limit $u = \sqrt{6}$ as the number of branches increases, which is significantly larger than the $\sqrt{3}$ value observed for arborescent polymers.[14] The $P(q)$ function derived by Benoit for star-branched polymers on the assumption of a Gaussian distribution of the chain elements is[16,17]

$$P(q) = \frac{2}{fv^4}\left(v^2 - (1 - \exp(-v^2)) + \frac{f-1}{2}(1 - \exp(-v^2))^2\right) \tag{4}$$

where f is the number of arms and $v = (f/(3f - 2))^{1/2}qR_g$. As the star becomes denser (increasing f), $u = q_{max}R_g$ is expected to decrease and reach a limit of $\sqrt{3.76}$, closer to $\sqrt{3}$.[14] The form factor $P(q)$ for hard spheres of uniform density in a SANS experiment is given by[18]

$$P(q) = \frac{9(\sin qR - qR\cos qR)^2}{(qR)^6} \tag{5}$$

where $R = \sqrt{5/3}R_g$ is the radius of the sphere. The form factor for hard spheres generates a maximum in the Kratky plots such that $q_{max}R_g \approx \sqrt{2.7}$. The Kratky R_g values determined according to eq 2 are in good agreement with the Guinier R_g values for the arborescent polystyrenes characterized regardless of generation number, branch size, and solvent quality (Tables 4 and 5). Uncertainties in R_g (Tables 4 and 5) were estimated by assuming an uncertainty of ±5% in q_{max}. As shown in Figure 2b, $u = \sqrt{3}$ determined for arborescent polymers is smaller than the value derived from the form factors for star- and AB_f-type hyperbranched polymers and approaches the hard sphere limit. This indicates that arborescent polymers are denser (more hard spherelike) than star and hyperbranched polymers.

The branching density of a branched polymer can be characterized by the contraction factor for its radius of gyration as compared to a linear polymer with the same molecular mass under Θ conditions.[19] This contraction factor is defined as

$$g = \frac{\langle R_g^2\rangle_b}{\langle R_g^2\rangle_l} \tag{6}$$

where the subscripts b and l refer to the branched and linear polymers, respectively. Equations for the g-factor under Θ conditions were derived by Zimm and Stockmayer for branched polymers with different architectures.[19] For polymers with branches of uniform size and randomly distributed branching points, the equation becomes

$$\langle g(m)\rangle_{Av} = [(1 + m/7)^{1/2} + 4m/9\pi]^{-1/2} \tag{7}$$

where m (≡ f_w in Table 1) corresponds to the total number of branching points per arborescent polymer molecule. The R_g predicted by the Zimm−Stockmayer model for G0−G3 5K arborescent polystyrenes was determined by combining eq 7 with the R_g of linear polystyrenes estimated from the equation $R_g = l\sqrt{N/6}$ where $l = 0.67$ nm and N is the number of monomer units corresponding to the same M_w as the arborescent polymers. As shown in Table 4, the R_g values calculated from the Zimm−Stockmayer equation agree well with those determined from the SANS measurements for arborescent polystyrenes with 5K side chains for all generations (G0−G3) in cyclohexane-*d*. The accurate predictions of the Zimm−Stockmayer model confirm that cyclohexane-*d* is a Θ-solvent at 30 °C for arborescent polystyrenes, in agreement with previous second virial coefficient measurements ($A_2 \approx 0$).[10]

The R_g of arborescent polystyrenes with longer (30K) side chains was determined as a function of generation number in cyclohexane-*d* ($T = 30$ °C, $\phi = 0.005$) for comparison to the polymers with 5K side chains. The dimensions of polymers with 30K side chains are obviously larger than for the ones with 5K side chains (Table 4). Even for the first-generation (G1) 30K polymer, R_g is already about the size of the third-generation (G3) 5K sample. In contrast to the 5K polymer series, the R_g values predicted by the Zimm−Stockmayer model are significantly larger than those measured for G0−G2 30K arborescent polymers in cyclohexane-*d*, as shown in Table 4. This indicates that the G0−G2 30K branched polymers have a denser, more compact structure than predicted by the randomly branched model of Zimm−Stockmayer. The scaling relation $R_g \propto M_w^{\nu}$ is compared for both series of arborescent polymer samples in Figure 3a. For arborescent polystyrenes with 5K branches, R_g

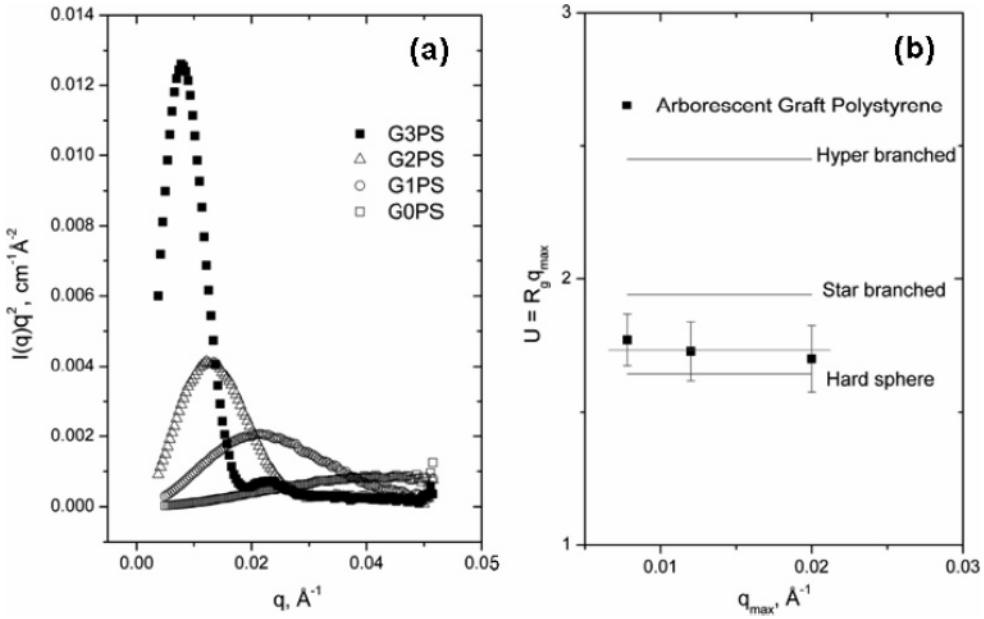

Figure 2. (a) Kratky plots for arborescent polystyrenes with 5K chains at $\phi = 0.005$ and $T = 30$ °C in CH-*d* (CH: cyclohexane); (b) comparison of u values predicted from the form factors for various systems with the experimental u value for arborescent polymers ($\phi = 0.005$ and $T = 30$ °C) in CH-*d*.

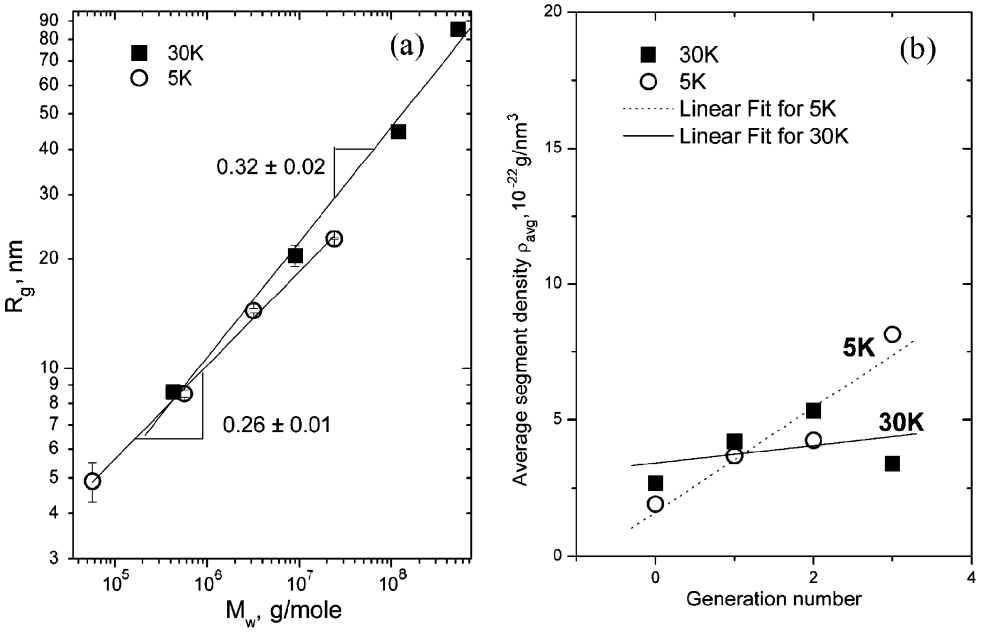

Figure 3. (a) Scaling relation for 5K (G0−G3) and 30K (G0−G3) arborescent polymers; (b) comparison of the average segment density ρ_{avg} for 5K vs 30K side chain materials in CH-*d*.

scales as $R_g \propto M_w^{\upsilon}$ where $\upsilon = 0.26 \pm 0.01$, in good agreement with $\upsilon = {}^1/_4$ predicted for the randomly branched model of Zimm−Stockmayer. This indicates that the average segment density increases with the size (or generation number) of the molecules for arborescent polymers with short (5K) side chains. In contrast, the samples with 30K branches have an exponent $\upsilon = 0.32 \pm 0.02$, much closer to the $\upsilon = {}^1/_3$ value expected for hard spheres,[20] which reflects an average segment density independent of size (generation number). This is mainly because of the drop in density for the 30K sample of generation 3 as shown in Figure 3b ($\rho_{avg} = 3M_w/4\pi R_g^3$). It is clear that the average density of the molecules increases linearly for successive generations of arborescent polymers with short (5K) side chains. The trend is much less obvious for samples with 30K side chains but can be approximated by a relatively flat line. The branching functionality (f_w) of the 30K samples increased 13-fold from G1 to G2 but only 4.3-fold for the G3 sample. The growth of the arborescent polymers may therefore have been limited in the grafting reaction by steric restrictions imposed by the finite volume of the larger 30K polymer chains and explain the lower density of the G3 sample. The same scaling factor $\upsilon = 0.32 \pm 0.02$ was also found in a good solvent (toluene-*d*) for the 30K polymers, confirming the hard spherelike behavior of the 30K polymers regardless of solvent quality. The scaling factor $\upsilon = 0.26 \pm 0.01$ observed for the 5K polymers is opposite to the normal fractal behavior of linear polymer chains and is intrinsically self-limiting. At the point where the density reaches a constant value (maximum chain packing attained), the scaling behavior should revert to $\upsilon = {}^1/_3$ for higher generations of 5K polymers. Such a crossover from $\upsilon = {}^1/_4$ to ${}^1/_3$ was predicted

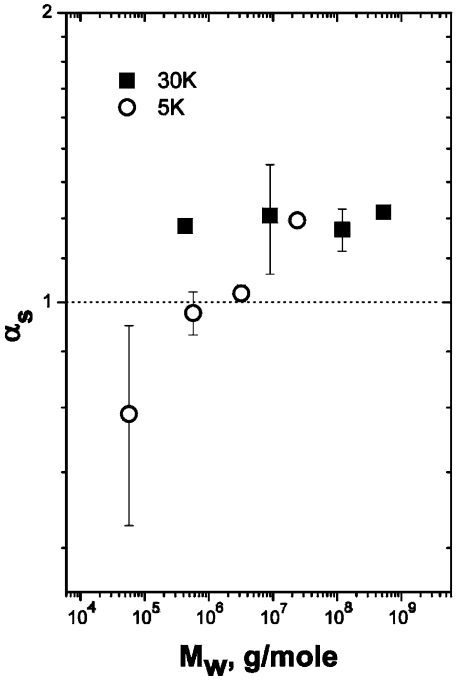

Figure 4. Comparison of expansion factor (α_s) for R_g measured for arborescent polymers with 30K and 5K side chains (good solvent, toluene-*d*; Θ solvent, CH-*d*).

by Stauffer and co-workers based on a percolation theory of gelation.[21,22] Similarly, a "starburst" limit of density growth for dendrimer molecules was also predicted by deGennes et al.[23] The scaling behavior $\upsilon \approx {}^1/_3$ observed for the 30K branched polymers (G1−G3) suggests that the self-limiting behavior is already observed at lower generations for these systems, due to greater steric restrictions imposed by the larger 30K chains. The influence of the solvent on R_g can be expressed in terms of the expansion factor α_s. The expansion factor due to excluded volume effects in a good solvent is usually defined as[24]

$$\alpha_s = \frac{(R_g)_{\text{goodsolvent}}}{(R_g)_{\Theta\text{solvent}}} \tag{8}$$

Toluene-*d* was used as a good solvent for arborescent polystyrenes. The α_s values determined are shown as a function of M_w (generation number) for both the 5K and 30K samples in Figure 4. For the 5K polymers, excluded volume effects were not clearly observed except for the G3 polymer ($\alpha_s > 1$). This suggests that the side chains in the 5K polymers have a partly stretched conformation regardless of solvent quality for lower generations (G1−G2), while the 30K polymers and the 5K polymers of higher M_w (generations) have a more coil-like conformation and a size changing with solvent quality. For linear polystyrenes,[25] in comparison, α_s scales with M_w according to the relation $\alpha_s \propto M_w^{1/5}$. The blob theory of branched polymers predicts a similar increase in α_s with the number of arms ($\alpha_s \propto f^{1/5}$).[26] Candau et al. likewise suggested that α_s should increase with the segmental density for branched polymers.[27] In contrast to the predictions of these theories for branched polymers, the relative independence of α_s on generation number for arborescent 30K polymers is attributed to their hard spherelike behavior. Since their average density is almost independent of M_w (and therefore independent of the generation number and branching functionality) in both good and Θ solvents, in agreement with the scaling relationship $R_g \propto M_w^{\upsilon}$ with $\upsilon \approx {}^1/_3$, α_s should also be essentially independent of M_w (or generation number) as observed experimentally.

Contrast Matching Experiments of PS-*graft*-PS-*d* Arborescent Copolymers. R_g Analysis by Guinier and Kratky Plots. The morphology of arborescent polymers was investigated further by SANS with the help of the contrast matching method. For this purpose, copolymers incorporating a protonated arborescent polystyrene core and a deuterated shell of polystyrene-*d* were synthesized (Tables 2 and 3). The polystyrene-*d* chains are randomly attached along the side chains of the substrate. Two arborescent polystyrene samples of overall generations G3 and G4 were thus obtained by grafting PS cores with PS-*d* side chains. These are identified as samples G2PS-*graft*-PS-*d* and G3PS-*graft*-PS-*d*, respectively. SANS measurements were carried out on dilute solutions of the copolymers ($\phi = 0.01$) in PS core-matching and PS-*d* shell-matching solvents. The R_g of the core is obtained in a shell-matching solvent, since the polymer chains in the shell are invisible (Figure 1b). When the solvent matches the core, the R_g determined from the SANS data represents the overall R_g of the hollow spheres. The composition of the protonated and deuterated solvent mixtures used as core- and shell-matching solvents for the polystyrene-*d* copolymers is provided in Table 5. The Guinier plots obtained in the core- and shell-matching solvents are shown in Figure 5a for G3 and G4 copolymers in THF and cyclohexane as typical good and Θ solvents for polystyrene, respectively. The R_g values derived from the Guinier analysis are provided in Table 5. The R_g values obtained by Kratky analysis (Figure 5b) using eq 2, also provided in Table 5, agree well with the Guinier analysis results for the core- and shell-matching conditions. Toluene-*d* has been used previously as a good solvent; however, the SLD of toluene-*d* (5.66×10^{-6} Å^{-2}) does not match PS-*d* (6.4×10^{-6} Å^{-2}) accurately and therefore THF/THF-*d* was used as an alternate good solvent. The quality of both solvents was similar, the R_g of the G3 polymer under core-matching conditions being 26.9 and 26.7 nm in THF and in toluene, respectively. The R_g for the G3 (G2PS-*graft*-PS-*d*) and G4 (G3PS-*graft*-PS-*d*) polymers in THF-*d* is larger than in cyclohexane-*d*, indicating an excluded volume effect in the good solvent. The expansion factors for the core and the shell were measured under the contrast matching method conditions. The α_s values of the cores are 1.03 ± 0.27 and 1.07 ± 0.27 for G3 and G4, respectively, which is smaller than $\alpha_s = 1.15 \pm 0.27$ and 1.13 ± 0.27 for the overall R_g (determined under core-matching conditions) of G3 and G4, respectively. This indicates that swelling is more significant for the shell than for the core. This seems reasonable because the side chains in the shell are only attached to the core substrate at one end, and therefore much more mobile than the chains in the core, where the branching points are distributed randomly along the chains. Comparison of $\alpha_s = 1.15 \pm 0.27$ and 1.13 ± 0.27 for the overall R_g of hollow spheres (determined under core-matching conditions) between G3 and G4, it seems that α_s for the 5K polymers with a high M_w remains constant and similar to α_s for the 30K samples.

Pair Distance Distribution Function $p(r)$ and Radial Density Profile $\rho(r)$. The scattering intensity $I(q)$ is related to the real space pair distance distribution function (PDDF) by the following Fourier transformation, which enables the determination of the overall shape and size of the scattering objects.[28]

$$I(q) = 4\pi \int_0^\infty p(r) \frac{\sin(qr)}{qr} \, \mathrm{d}r \tag{9}$$

The direct Fourier transformation method requires scattering data in the full q range, $0 < q < \infty$. The finite q range available from an experiment would lead to strong oscillations (termina-

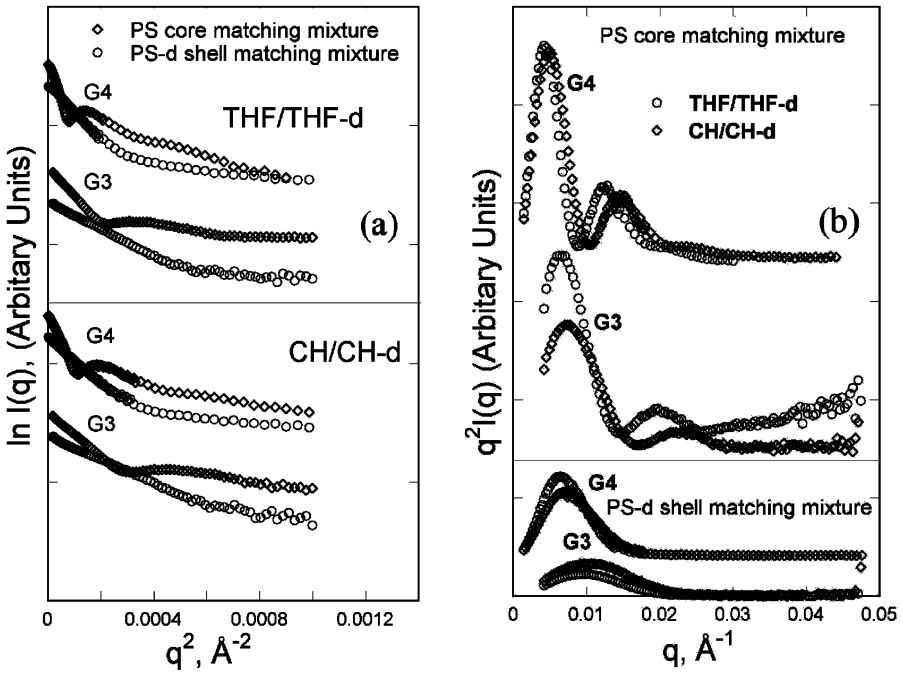

Figure 5. (a) Guinier plots and (b) Kratky plots for SANS data from the core and the shell of G2PS-*graft*-PS-*d* and G3PS-*graft*-PS-*d* ($\phi = 0.01$) in THF 80%/THF-*d* (shell-matching), THF-*d* (core-matching), CH 0.4%/CH-*d* (shell-matching), and CH 76%/CH-*d* (core-matching).

Table 5. Radii of Gyration Measured for Polystyrene-*d* Copolymers by Guinier and Kratky Analyses of the SANS Data

		G2PS−PS-*d* R_g (nm)		G3PS−PS-*d* R_g (nm)	
	solvent (ϕ)	Guinier	Kratky	Guinier	Kratky
shell-matching	THF-*d*	18.9 ± 2.1	18.8 ± 0.9	26.1 ± 3.5	28.4 ± 1.4
core-matching	THF(0.8)/THF-*d*	26.9 ± 1.6	26.2 ± 1.3	41.0 ± 5.9	42.3 ± 2.1
shell-matching	cyclohexane (0.04)/cyclohexane-*d*	18.3 ± 2.8	17.3 ± 0.9	24.4 ± 1.6	24.7 ± 1.2
core-matching	cyclohexane (0.76)/cyclohexane-*d*	23.5 ± 2.2	24.4 ± 1.2	36.4 ± 3.0	37.7 ± 1.9

tion effect) in a direct Fourier transformation. These termination effects can be minimized by the indirect Fourier transformation (IFT) method. The PDDF is also related to a scattering length density (SLD) $\rho(r)$ as[29]

$$p(r) = r^2 \int_{-\infty}^{\infty} \rho(\bar{r})\rho(\bar{x} - \bar{r})\mathrm{d}\bar{x} \qquad (10)$$

In the case of high symmetry (sphere, cylinder, or lamella), the PDDF can be deconvoluted to obtain the scattering length density profile. The generalized indirect Fourier transformation (GIFT) and deconvolution calculations on the SANS data from the arborescent polystyrene solutions were performed with the programs GIFT[30,31] and DECON,[32−34] respectively. The particle interactions can be considered negligible because the volume fraction of arborescent polystyrenes is below 1%. In fact, taking into account the structure factor in fitting the data with the GIFT program did not change the final result for $p(r)$, so no structure factor was considered in data analysis. The arborescent polymers studied here have about 10% polydispersity, as shown in Tables 1−3. The PDDF obtained from the experimental data by the IFT method contains not only information on the shape and structure of the molecules but also their polydispersity and deviation from high symmetry. It is possible to perform the deconvolution calculations for various assumed size distributions using DECON, and the one that is closest to the real polydispersity will give the best fit to $p(r)$.[34] The deviation from high symmetry can also affect the PDDF, but this was ignored in deconvoluting $p(r)$ to the scattering length density profile.

As shown in Figures 6a, 7a, and 8a, applying the IFT method resulted in very good fit to the experimental data for G3 and G4 copolymers in the various ratios of THF/THF-*d*. Figure 6a shows the SANS data and the fits by the IFT method for the core (shell contrast matching in THF/-THF-*d*). The corresponding pair distance distribution function and excess SLD (contrast) profiles are shown in Figure 6b,c. The shape of the PDDF obtained for the core of the G3 and G4 copolymers (when the shell of the copolymers has the same scattering length as the solvent) is typical of spherical structures. The PDDF vanishes at the maximum diameters (550 and 840 Å), corresponding to the size of the G2 and G3 polystyrene homopolymers previously measured in dynamic light scattering and viscosity experiments. The excess SLD profiles obtained by deconvolution of the PDDF agree with the polymer density profile calculated by fitting the SANS data with a form factor corresponding to a shape where $\rho(r)$ is maximum at the center of a molecule and decays as a function of r (the radial distance from the center of the molecule) according to a power law function.[10,11] For arborescent polymers, branching points are uniformly distributed throughout the molecule as the branching density increases. In contrast to the random and uniform distribution of branching points of arborescent polymers, a dendrimer has the same branching functionality as the monomer units at the end of the previous generation. The "starburst limit" already discussed in the previous section of this paper refers specifically to the limit of further growth due to the "dense shell" of the dendrimer. From this model, based on the geometry of the branching point distribution and assuming ideally rigid monomer units, a dense shell and hollow core picture has been suggested for the density profile of dendrimers. In contrast, recent theoretical and

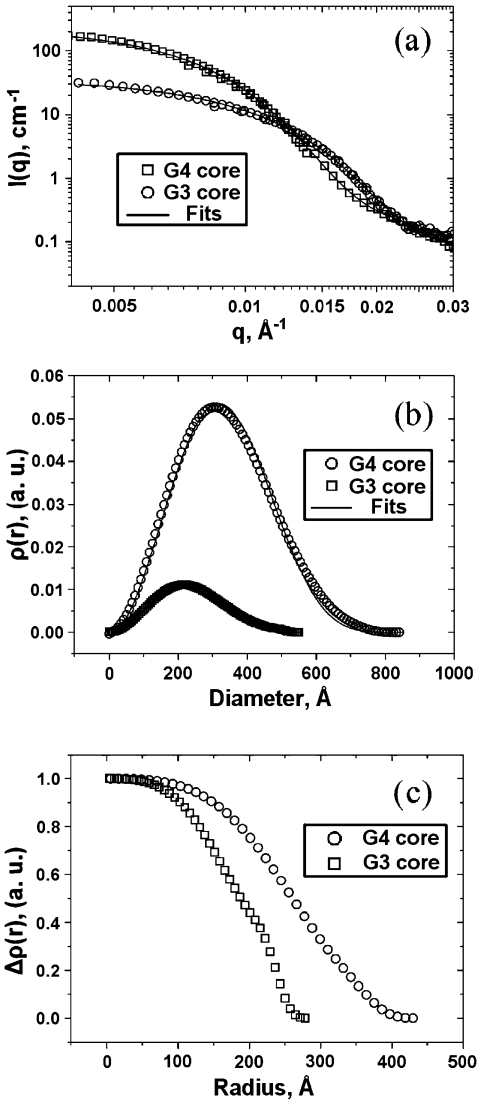

Figure 6. (a) Experimental SANS data and fits by the IFT method using the GIFT program for the core of G2PS-*graft*-PS-*d* and G3PS-*graft*-PS-*d* (shell contrast matching in THF/THF-*d*); (b) corresponding PDDF and (c) contrast profiles ($\Delta\rho(r)$) of polymers deconvoluted by the DECON program. The solid lines in part b are the fitted curves for the deconvolution calculations by the DECON program to obtain the contrast profiles $\Delta\rho(r)$. A 5% polydispersity assuming a Schultz distribution was used for the deconvolution calculations, and the $\rho(r)$ values were normalized to a maximum = 1.

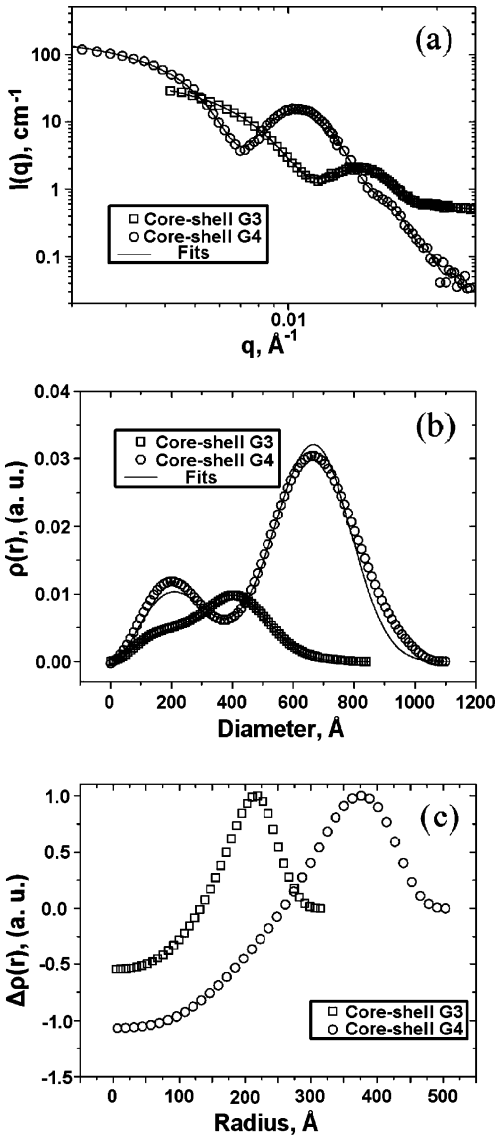

Figure 7. (a) Experimental SANS data and fits by the IFT method using the GIFT program for G2PS-*graft*-PS-*d* and G3PS-*graft*-PS-*d* in THF/THF-*d*, 50/50 (intermediate contrast between the PS core and the PS-*d* shell); (b) corresponding PDDF and (c) contrast profiles ($\Delta\rho(r)$) of polymers deconvoluted by the DECON program. The solid lines in part b are the fitted curves for the deconvolution calculations by the DECON program to obtain the contrast profiles $\Delta\rho(r)$. A 20% polydispersity assuming a Schultz distribution was used for the deconvolution calculations, and the $\rho(r)$ values were normalized to a maximum = 1.

experimental studies of flexible dendrimers in solution have demonstrated that the density profile actually has its maximum at the center due to significant back-folding of the outer groups into the center of the molecules.[35,36] Back-folding of the shell chains of arborescent polymers may also occur and be responsible for the maximum density profile at the center. However, the "dense sphere" morphology of the G2 and G3 core substrates due to their high branching density may well hinder the shell chains from back-folding into the core space. The question of the presence of a thick core−shell interfacial region rather than a well-defined core phase, due to the random distribution of branching points within arborescent polymer molecules, was also considered previously.[11] A well-defined core−shell structure would imply that most of the PS and PS-*d* are reasonably well-separated (exclusively located) in the core and the shell regions, respectively. If arborescent copolymers have a well-defined core−shell morphology and the solvent has a scattering length density value intermediate between the PS core (1.4×10^{-6} Å^{-2}) and the PS-*d* shell (6.4×10^{-6} Å^{-2}), the scattering profile should show the characteristics of inhomogeneous spheres with a difference in core and shell scattering contrasts. An intermediate SLD value for the solvent (3.9×10^{-6} Å^{-2}) was achieved with a THF/THF-*d* (50/50) mixture. The PDDF for the G3 and G4 copolymers in THF/THF-*d* (50/50) are shown in Figure 7b. The obtained PDDF have a shape typical of concentric (core−shell) spheres where the core and shell scattering contrasts are different. The maximum diameters of the PDDF correspond to the size measured by dynamic light scattering. The G4 molecules, in particular, display two distinctive maxima indicating better phase separation between the core and the shell regions as compared to G3. The neutron SLD contrast profiles (Figure 7c) show two regions of opposite signs: the inner part of the arborescent polymers with a negative scattering contrast and the outer part with a positive contrast.

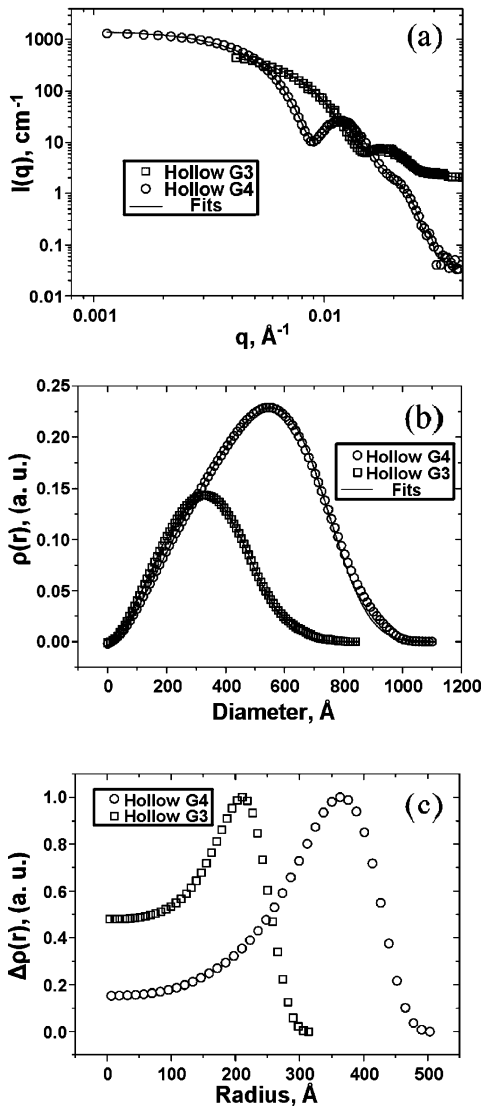

Figure 8. (a) Experimental SANS data and fits by the IFT method using the GIFT program for the hollow sphere of G2PS-*graft*-PS-*d* and G3PS-*graft*-PS-*d* (core contrast matching in THF/THF-*d*); (b) corresponding PDDF and (c) contrast profiles ($\Delta\rho(r)$) of polymers deconvoluted by the DECON program. The solid lines in part b are the fitted curves for the deconvolution calculations by the DECON program to obtain the contrast profiles $\Delta\rho(r)$. A 10% polydispersity assuming a Schultz distribution was used for the deconvolution calculations, and the $\rho(r)$ values were normalized to a maximum = 1.

This result clearly shows that the core mostly consists of PS and the shell of PS-*d*. The relatively higher values of the density profile for the G3 core region as compared to G4 shown in Figure 7c indicates that the PS-*d* of higher SLD penetrates the core region more deeply. Figure 8b shows the PDDF and excess SLD profiles for the hollow spheres (shells). As anticipated for a well-defined core−shell morphology, the density profile obtained in Figure 8c is close to that of a hollow sphere. Only a small amount of PS-*d* exists within the core region for the G4 molecules. This indicates that the chains in the shell (introduced in the final grafting reaction) do not reach significantly into the G3 core. In contrast, a significant amount of PS-*d* is present within the core for the lower generation G3 copolymer. This is probably because the PS core of the G3 molecules is smaller and less dense, and the distance between the chains in the shell and the center is much smaller than in the G4 molecules. As a result, any back-folding of the shell chains may allow them to reach the core region more effectively as compared to the higher generation G4 molecules.

Conclusions

The R_g values determined by Guinier analysis and from the maximum in the Kratky plots using $q_{max}R_g = \sqrt{3}$ are self-consistent. The scaling factor υ ($R_g \propto M_w^{\upsilon}$) of G0−G3 polymers was found to be $\upsilon = 0.26 \pm 0.01$ for 5K and 0.32 ± 0.02 for 30K polymers, in agreement with the values predicted for randomly branched polymers by the Zimm−Stockmayer model and the hard sphere model, respectively. The expansion factor (α_s) for R_g in a good solvent remained relatively constant over successive generations of 5K (G3 and G4) and 30K (G0−G3) polystyrenes. The SANS contrast matching method allowed detailed profiling of the radial segment density within the core and shell phases of arborescent PS-*graft*-PS-*d* copolymers. The higher generation G3PS-*graft*-PS-*d* copolymer had a better-defined core−shell structure than the lower generation G2PS-graft-PS-*d* copolymer.

Acknowledgment. This work has benefited from the use of the 30 m NIST-NG3 and NIST-NG7 instruments at the Center for Neutron Research at the National Institute of Standards and Technology. We acknowledge the support of the National Institute of Standards and Technology, U.S. Department of Commerce, in providing the neutron research facilities used in this experiment. This research was supported in part by an appointment to the ANSTO Postdoctoral Research Associate Program. The financial support of the Natural Sciences and Engineering Research Council of Canada is acknowledged for the synthetic part of the work.

References and Notes

(1) Teertstra, S. J.; Gauthier, M. *Prog. Polym. Sci.* **2004**, *29*, 277.
(2) Voit, B. *J. Polym. Sci., Part A: Polym. Chem.* **2000**, *38*, 2505.
(3) Kim, Y. H. *J. Polym. Sci., Part A: Polym. Chem.* **1998**, *36*, 1685.
(4) Tomalia, D. A. *Aldrichimica Acta* **2004**, *37*, 39.
(5) Kawaguchi, H. *Prog. Polym. Sci.* **2000**, *25*, 1171.
(6) Gauthier, M.; Li, W.; Tichagwa, L. *Polymer* **1997**, *38*, 6363.
(7) Striolo, A.; Prausnitz, J. M.; Bertucco, A.; Kee, R. A.; Gauthier, M. *Polymer* **2001**, *42*, 2579.
(8) Gauthier, M.; Tichagwa, L.; Downey, J. S.; Gao, S. *Macromolecules* **1996**, *29*, 519.
(9) Kee, R. A.; Gauthier, M. *Macromolecules* **2002**, *35*, 6526.
(10) Choi, S.; Briber, R. M.; Bauer, B. J.; Topp, A.; Gauthier, M.; Tichagwa, L. *Macromolecules* **1999**, *32*, 7879.
(11) Yun, S. I.; Briber, R. M.; Kee, R. A.; Gauthier, M. *Polymer* **2003**, *44*, 6579.
(12) *NG3 and NG7 30-Meter SANS Instruments Data Acquisition Manual*; National Institute of Standards and Technology Cold Neutron Research Facility, 1996.
(13) Glinka, C. J.; Barker, J. G.; Hammouda, B.; Krueger, S.; Moyer, J. J.; Orts, W. J. *J. Appl. Crystallogr.* **1998**, *31*, 430.
(14) Burchard, W. *Macromolecules* **1977**, *10*, 919.
(15) Hedden, R. C.; Bauer, B. J. *Macromolecules* **2003**, *36*, 1829.
(16) Cassassa, E. F.; Berry, G. C. *J. Polym. Sci., Part A-2* **1966**, *4*, 881.
(17) Benoit, H. *J. Polym. Sci.* **1953**, *11*, 506.
(18) Roe, R.-J. *Methods of X-Ray and Neutron Scattering in Polymer Science*; Oxford University Press: New York, 2000.
(19) Zimm, B. H.; Stockmayer, W. H. *J. Chem. Phys.* **1949**, *17*, 1301.
(20) The term "hard sphere" in this context does not refer to a uniform distribution of chain segments throughout the molecules but rather to dense spheres having a constant average density for successive generations (or increasing M_w).
(21) Stauffer, D. *Phys. Rep.* **1979**, *54*, 1.
(22) Stauffer, D. *Pure Appl. Chem.* **1981**, *53*, 1479.
(23) de Gennes, P. G.; Hervet, H. *J. Phys., Lett.* **1983**, 351.
(24) Flory, P. J. *Principles of Polymer Chemistry*; Cornell University Press: Ithaca, NY, 1953.
(25) Miyaki, Y.; Einaga, Y.; Fujita, H. *Macromolecules* **1978**, *11*, 1180.
(26) Daoud, M.; Cotton, J. P. *J. Phys. (Paris)* **1982**, *43*, 531.
(27) Candau, F.; Rempp, P.; Benoit, H. *Macromolecules* **1972**, *5*, 627.
(28) Glatter, O. *J. Appl. Crystallogr.* **1979**, *12*, 166.

(29) Glatter, O. *J. Appl. Crystallogr.* **1980**, *13*, 7.
(30) Brunner-Popela, J.; Glatter, O. *J. Appl. Crystallogr.* **1997**, *30*, 431.
(31) Weyerich, B.; Brunner-Popela, J.; Glatter, O. *J. Appl. Crystallogr.* **1999**, *32*, 197.
(32) Glatter, O. *J. Appl. Crystallogr.* **1981**, *14*, 101.
(33) Glatter, O.; Hainisch, B. *J. Appl. Crystallogr.* **1984**, *17*, 435.
(34) Mittelbach, R.; Glatter, O. *J. Appl. Crystallogr.* **1998**, *31*, 600.
(35) Ballauff, M. *Top. Curr. Opin.* **2001**, *212*, 177.
(36) Rosenfeldt, S.; Dingenouts, N.; Ballauff, M.; Werner, N.; Vögtle, F.; Linder, P. *Macromolecules* **2002**, *35*, 8098.

MA7021106